The role of electron dissipation on the rate of collisionless magnetic reconnection

M. A. Shay and J. F. Drake

Institute for Plasma Research, University of Maryland, College Park, MD 20742

Abstract. Particle simulations and analytic arguments are presented to demonstrate that the electron dissipation region, including the physics which breaks the frozen-in condition, does not affect the rate of reconnection in collisionless plasma. The result is a general consequence of the quadratic nature of the dispersion character of whistler waves, which control the plasma dynamics at small scales. The reconnection rate is instead controlled by the dynamics at length scales much greater than the electron dissipation region.

Introduction

Magnetic reconnection plays an important role in the dynamics of the magnetosphere, the solar corona, and laboratory experiments by allowing magnetic energy to be released in the form of high velocity streams of electrons and ions. In resistive magnetohydrodynamic (MHD) models of this process, resistivity breaks the frozen-in constraint in a boundary layer called the dissipation region allowing reconnection to occur. At low values of resistivity the dissipation region forms a macroscopic Sweet-Parker layer which severely limits the rate of reconnection [*Sweet*, 1958; *Parker*, 1957; *Biskamp*, 1986], the inflow velocity into the magnetic X-line scaling like

$$v_i \sim \frac{\delta}{L} c_A \ll c_A, \qquad (1)$$

with δ and L being, respectively, the small, resistivity-dependent width and macroscopic length of the dissipation region and c_A being the Alvén velocity. As resistivity goes to zero, $\delta \to 0$ and reconnection proceeds only in the presence of anomalous resistivity [*Biskamp*, 1993]. In physical systems of interest, resistivity is too weak to explain the observations and anomalous resistivity remains poorly understood.

In collisionless plasma the dissipation region develops a multiscale structure based on electron and ion scale lengths [*Biskamp et al.*, 1997; *Shay et al.*, 1998]. Within a distance of the order of the ion inertial length $\delta_i = c/\omega_{pi}$ the ion motion decouples from that of the electrons[*Mandt et al.*, 1994] and the magnetic field and the ions are accelerated away from the X-line, eventually reaching the Alfvén velocity. Within this ion inertial region but outside of an electron inertial region, the electrons remain frozen-in to the magnetic field and the dynamics of the electron magnetofluid are described by a set of nonlinear whistler equations [*Mandt et al.*, 1994; *Biskamp et al.*, 1997]. Finally, even closer to the X-line the electrons decouple from the magnetic field either as a result of their

finite thermal velocity [*Laval et al.*, 1966] or their convective motion [*Dungey*, 1988; *Burkhart et al.*, 1990]. In a fluid description the mechanism for breaking the electron frozen-in condition can be described either as electron inertia or a non-gyrotropic pressure [*Vasyliunas*, 1975] and has recently been the subject of intense scrutiny [*Lyons and Pridemore-Brown*, 1990; *Cai et al.*, 1994; *Biskamp et al.*, 1997; *Horiuchi and Sato*, 1997; *Shay et al.*, 1998; *Kuznetsova et al.*, 1998; *Hesse and Winske*, 1998].

Since the early explorations of the mechanism for breaking the frozen-in flux condition, it was recognized that during steady state reconnection electron inertia cannot balance the reconnection electric field at the X-line since in a 2-D model the flows vanish at this location [*Vasyliunas*, 1975]. In seeming contradiction to these results, however, studies of 2-D steady-state reconnection using only electron inertia to break the frozen-in constraint find that not only is steady-state reconnection possible, but that the reconnection rate is independent of electron inertia [*Biskamp et al.*, 1997; *Shay et al.*, 1998]. In hybrid and Hall MHD simulations in which resistivity breaks the frozen-in condition, the reconnection rates are similarly insensitive to the actual values of resistivity used in the simulations [*Mandt et al.*, 1994; *Ma and Bhattacharjee*, 1996].

The underlying physics is linked to the different dispersion character of the whistler and Alfvén waves. In all of the simulations which include the Hall effect, the structure of the electron inertial region is controlled by whistler rather than Alfvén dynamics because this region has an intrinsic scale length which is well below the ion inertial length. The quadratic dispersion character of the whistler wave ($\omega \sim k^2$) leads to an increase in the phase speed with decreasing scale size and therefore to an increase in the velocity at which the electrons can be ejected from the X-line as the scale size of the electron dissipation region decreases. The consequence is that, in contrast to the resistive MHD scaling in Eq. (1), the whistler dynamics leads to an inflow velocity which is independent of the width of the dissipation region. This can be shown by carrying out a Sweet-Parker-like analysis of the dissipation region using the whistler equations. We take the width of the layer in the inflow (z) direction, δ, to be controlled by an unspecified mechanism which breaks the electron frozen-in condition, and the length in the outflow (x) direction to be $L \gg \delta$. In the whistler regime the electrons are frozen-in to the magnetic field and the ion motion can be neglected. The resulting dynamical equations in a 2-D system are[*Biskamp et al.*, 1997]

$$\frac{\partial \psi}{\partial t} + \mathbf{v}_e \cdot \nabla \psi = 0, \quad \frac{\partial B_y}{\partial t} - \mathbf{B} \cdot \nabla v_{ey} = 0 \qquad (2)$$

$$\mathbf{v}_e = -\frac{c}{4\pi ne} (\nabla B_y \times \hat{y} + \hat{y}\nabla^2 \psi) \qquad (3)$$
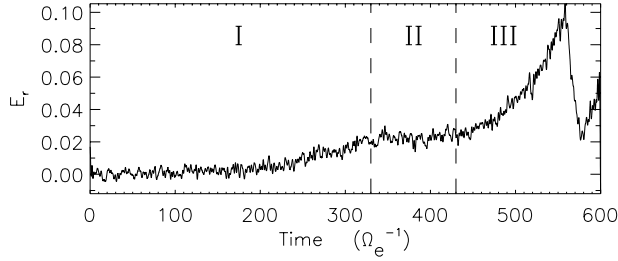
Figure 1. Reconnection electric field E_r versus time for $L_x = 80$.

where $\mathbf{B} = \hat{y} \times \nabla\psi + B_y\hat{y}$. The outflow velocity follows from the x component of (3), $v_{ex} \sim cB_y/(4\pi ne\delta)$. The out-of-plane field B_y arises from bending the in-plane field. The source $(\sim B_x v_{ey}/L)$ acts for a time of the order of the convection time out of the dissipation region $\sim L/v_{ex}$ so $B_y \sim B_x v_{ey}/v_{ex}$. Combining these relations and eliminating v_{ey} using (3), we obtain $B_y \sim B_x$, $v_{ex} \sim v_{ey}$ and the electron outflow velocity $v_{ex} \sim \Omega_e\delta_e^2/\delta$, which is the whistler analogue of the Alfvén outflow condition in MHD. The important point is that this outflow velocity scales inversely with the width of the dissipation region. Applying continuity ($v_{ex}\delta \sim v_iL$), the inflow velocity is given by

$$v_i \sim \frac{1}{L}\delta_e^2\Omega_e. \qquad (4)$$

The reconnection rate is independent of δ and therefore the mechanism by which the electron frozen-in condition is broken. The reconnection rate remains finite even as $\delta \to 0$. In fact, the reconnection rate given in (4) is sufficiently large (it will turn out that L is actually microscopic) that the whistler time of the global system is more of a constraint on the reconnection rate; consequently, the electron dissipation region has no impact on the rate of reconnection.

In this paper, we focus on the structure of the electron dominated inner layer of the dissipation region where whistler physics and electron inertial dynamics are important but where the ions play no significant role. Using an electron particle code we are able to explore the relative roles of inertia and the non-gyrotropic pressure in breaking the frozen-in condition and are able to demonstrate that the microphysics associated with these processes have no impact on the reconnection rate. Instead, it is the large scale macroscopic physics which controls this rate, in this case the global whistler dynamics. In a simulation including the ions, it would be the dynamics of the ion dissipation region.

Particle Simulation Model

This study is performed with a 2 1/2 dimensional electron particle-in-cell (PIC) code. The ions constitute a stationary background of density n_0. This allows us to focus on the dynamics of whistlers and the electron dissipation region without the problems arising from inadequate separation of scales due to unrealistic ion to electron mass ratios. The electric and magnetic fields are stepped forward using the full Maxwell's equations. At the end of each time step, the electric field is modified by adding an electrostatic component to insure that $\nabla \cdot \mathbf{E} = 4\pi\rho$. Time is normalized to the electron cyclotron time Ω_e^{-1}, based on the max-
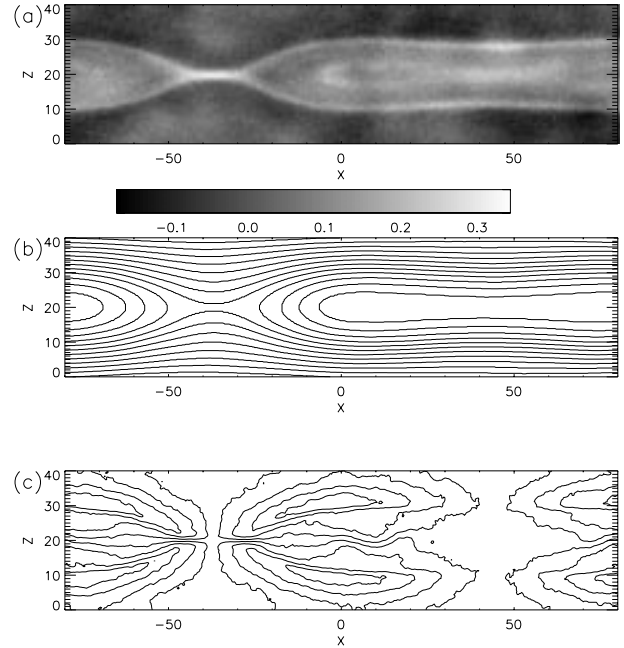

Figure 2. The (a) out-of-plane electron current J_y, (b) flux function ψ, and (c) out-of-plane magnetic field B_y for $L_x = 160$.

imum initial magnetic field B_0. Length scales are normalized to c/ω_{pe} based on n_0. Velocity is therefore normalized to $c_{Ae} = \sqrt{B_0^2/(4\pi n_0 m_e)}$. The speed of light, c, is equal to $5c_{Ae}$ for all simulations. The Debye length is only marginally resolved.

The initial configuration of the system is a double current sheet in the (x, z) plane in a box of length L_x and width L_z, with $L_x/L_z = 2$. The boundary conditions are periodic in both directions. The initial current sheets are located at $z = \pm L_z/4$ with the initial magnetic field given by $B_x = \tanh[(z + L_z/4)/w_0] - \tanh[(z - L_z/4)/w_0] - 1$. Small magnetic perturbations and associated currents are added to form seed magnetic islands centered around the two current layers. The grid scales, Δ_x and Δ_z, are 0.3125.

Unlike a conventional Harris equilibrium in which the variation of the density produces the equilibrium current, we take the density to be nearly constant, the current being produced by the $\mathbf{E} \times \mathbf{B}$ drift of electrons. The temperature T_e is spatially uniform. There are on average 50 particles/cell initially loaded with a shifted gaussian consistent with the equilibrium density and current. The largest simulation is 512×256 grid points with 7 million particles. For this series of simulations, we varied L_x and L_z, m_e, w_0, and T_e. The growth of magnetic islands in this system is robust and proceeds without saturation so that the quasi-steady reconnection rate and associated structure of the current layer can be studied as a function of critical parameters.

Simulation Results

Figure 1 is a plot of the reconnection electric field, E_y at the x-line, versus time for $L_x = 80$. During time period I, the x-lines form and the reconnection rate increases to
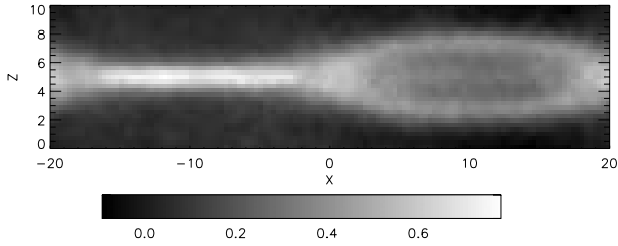
Figure 3. The out-of-plane electron current J_y for $L_x = 40$.

Figure 4. Reconnection electric field E_r versus: (a) the macroscopic system length L_x at fixed electron mass, and (b) the electron mass at fixed L_x.

its quasi-steady value. During time period II, reconnection is quasi-steady and will be the focus of our analysis. In time period III, the flux bubbles have grown so that they nearly reach the X-lines of the adjacent current layer and this causes a sudden enhancement of the reconnection rate.

Figure 2 shows the out-of-plane electron current, in-plane magnetic field lines, and out-of-plane magnetic field B_y during the quasi-steady reconnection period from a simulation with $L_x = 160$. To save space, only half of the simulation box is shown in Figures 2 and 3. The structure of the electron current layer around the magnetic x-line has reached a quasi-steady state, its width and length being independent of the width of the initial current layer. Consistent with the earlier fluid simulations [*Biskamp et al.*, 1997; *Shay et al.*, 1998], the electron current layer is microscopic in both the inflow and outflow directions, that is, it is not of the order of the macroscale, L_x, as in MHD. This can be more clearly seen by comparing the current layer in Fig. 2a with that from a simulation with $L_x = 40$ in Fig. 3. The basic scale lengths of the layer are almost unchanged in spite of the substantial difference in L_x. The out-of-plane field B_y represent the approximate streamlines of the electron flow since for c large, the in-plane current is given approximately by $\nabla B_y \times \hat{y}$. The presence of B_y is a signature of the whistler dynamics.

Figure 4a is a plot of the reconnection electric field, E_r, versus $1/L_x$ which demonstrates that $E_r \propto 1/L_x$. This scaling implies that reconnection is controlled by the global whistler time of the system and not the electron dissipation region. The global whistler time scales like L_x^2 and the magnetic flux in the system scales like L_x. Thus, E_r scales like the total flux divided by the time, or like $1/L_x$. To make the absence of a dependence on the electron dissipation region more explicit, we can rescale the data shown in Fig. 4a so that we vary the electron mass at a fixed system size. The results in Fig. 4b demonstrate that the reconnection rate is independent of the electron mass and therefore independent of the dynamics of the electron dissipation region, as found in previous two fluid [*Biskamp et al.*, 1997] and hybrid [*Shay et al.*, 1998] simulations. Finally, the reconnection rate is insensitive to the electron temperature, which has been varied by a factor of sixteen, and the initial current layer width, which has been varied by a factor of two. Thus, reconnection rate does not depend on the physics that breaks the electron frozen-in constraint.

The width of the current layer in the inflow direction is controlled by the Larmor radii of the unmagnetized electrons as they bounce back and forth across the x-line [*Laval et al.*,
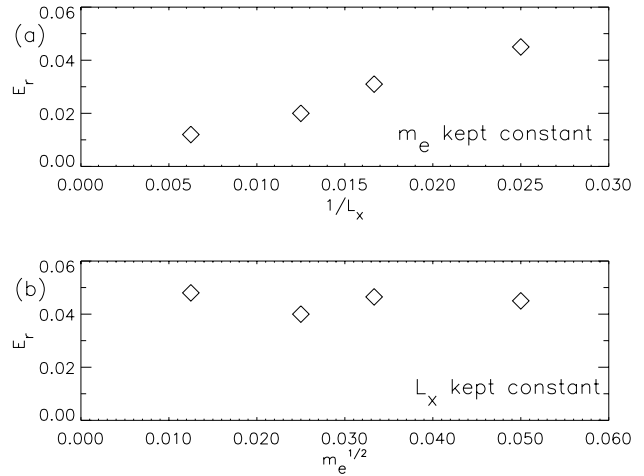
1966; *Horiuchi and Sato*, 1997]. This width is always of the order of c/ω_{pe}, but its exact value varies with the inflow thermal velocity v_{te} of the electrons. The turning point δ of electrons being reflected from the magnetic field B_x on either side of the x-line is given by [*Laval et al.*, 1966]

$$\delta \sim \sqrt{\frac{v_{te}}{\Omega'_{ex}}}, \qquad (5)$$

where $\Omega'_{ex} = \partial\Omega_{ex}/\partial z$. Figure 5 is a plot of this expression with Ω_{ex} measured from the simulations versus the measured width w of the electron current layer. At sufficiently low thermal velocities the current layer width should approach a constant in which v_{te} is replace by the $\mathbf{E} \times \mathbf{B}$ inflow velocity $cE_y/B_x(\delta)$ [*Dungey*, 1988; *Burkhart et al.*, 1990]. Unfortunately, we cannot demonstrate this transition due to heating from density fluctuations.

The electron outflow velocity is much greater than the inflow velocity, typically being comparable to or sometimes larger than the thermal velocity. This is because the upper limit on the outflow velocity of electrons is the peak whistler speed or the electron Alfvén velocity c_{Ae}, which typically exceeds the electron thermal velocity. The fluid picture of the acceleration of electrons and their ejection from the current layer is therefore relevant [*Dungey*, 1988; *Burkhart et al.*, 1990]. On entry into the unmagnetized region, electrons
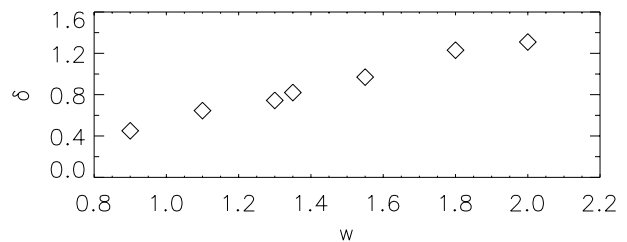

Figure 5. Predicted width of the electron current layer δ versus the measured current layer width w.

are accelerated in the y direction by the reconnection electric field E_r. The magnetic field B_z causes the particles to rotate into the outflow direction. Therefore, the outflow velocity v_x is comparable and scales the same as the out-of-plane velocity v_y; the length of the current layer in the x direction, Δ, is basically the effective Larmor radius based on these velocities; and the time that a fluid element spends in the current layer is given by $t_c \sim (\partial \Omega_z/\partial x \; \Delta)^{-1}$. Putting this picture together, v_x, v_y and Δ scale like [*Dungey*, 1988; *Burkhart et al.*, 1990]

$$v_y \sim v_x \sim \left(\frac{eE_r}{m_e}\right) t_c \sim \left(\frac{eE_r}{m_e}\right)^{2/3} \frac{1}{(\partial\Omega_z/\partial x)^{1/3}}, \quad (6)$$

$$\Delta \sim \left(\frac{eE_r}{m_e}\right)^{1/3} \frac{1}{(\partial\Omega_z/\partial x)^{2/3}}. \quad (7)$$

Equation (6) implies that the integrated current in the electron layer, and therefore the jump in B_x across this current layer, should decrease with increasing system size L_x since $E_r \propto 1/L_x$ and therefore $v_y \propto 1/L_x^{2/3}$. As L_x becomes larger, the electron current sheet weakens, which has been confirmed in these simulations. Finally, Eqn. (7) predicts that the length of the electron current layer is microscopic and actually decreases slightly with increasing system size. This is also consistent with the current layers shown in Figs. 2a and 3. We emphasize that the thermal velocities are comparable to the fluid velocities in the simulations so no simple theory quantitatively describes the simulation results.

Conclusion

The results presented demonstrate that the reconnection rate in collisionless plasma is insensitive to the mechanism which breaks the electron frozen-in condition in the collisionless particle description of the dynamics. This result is consistent with the hybrid and two fluid models and is a consequence of the quadratic nature of the whistler frequency. The results imply that a Hall MHD model of the magnetosphere should adequately describe the dynamics of reconnection once the linear phase of reconnection has past. It remains to be seen whether a fluid model can adequately describe the onset of the expansion phase of substorms, which may depend on the onset of kinetic instabilities.

References

Biskamp, D., Magnetic reconnection via current sheets, *Phys. Fluids, 29,* 1520, 1986.

Biskamp, D., and U. Bremer, Dynamics and Statistics of Inverse Cascade Processes in 2D Magnetohydrodynamics Turbulence, *Phys. Rev. Lett. 72,* 3819, 1993.

Biskamp, D., E. Schwarz, and J. F. Drake, Two-fluid theory of collisionless magnetic reconnection, *Phys. Plasmas, 4,* 1002, 1997.

Burkhart, G. R., J. F. Drake, and J. Chen, Magnetic Reconnection in Collisionless Plasmas: Prescribed Fields, *J. Geophys. Res., 95,* 18833, 1990.

Cai, H. .J., D. Q. Ding, and L. C. Lee, Momentum transport near a magnetic X line in collisionless reconnection, *J. Geophys. Res., 99,* 35, 1994.

Dungey, J. W., Noise-free neutral sheet, in Proceedings of an International Workshop in Space Plasma, vol. II, *Eur. Space Agency Spc. Publ.*, ESA SP-285, 15, 1988.

Hesse, M., and D. Winske, Electron Dissipation in collisionless Magnetic Reconnection, *J. Geophys. Res.,* in press, 1998.

Horiuchi, R., and T. Sato, Particle simulation study of collisionless driven reconnection in a sheared magnetic field, *Phys. Plasmas, 4,* 277, 1997.

Laval, G. R., R. Pellat, and M. Vuillemin, Instabilities electromagnetiques des plasmas sans collisions, *Plasma Phys. Controlled Nucl. Fusion Res., 2,* 259, 1966.

Kuznetsova, Masha M., M. Hesse and D. Winske, Kinetic Quasi-Viscous and Bulk Flow Inertia Effects in Collisionless Magnetotail Reconnection, *J. Geophys. Res., 103,* 199, 1998.

Lyons, L. R., and D. C. Pridemore-Brown, Force balance near an X line in a collisionless plasma, *J. Geophys. Res., 95,* 20903, 1990.

Ma, Z. W., and A. Bhattacharjee, Fast impulsive reconnection and current sheet intensification due to electron pressure gradients in semi-collisional plasmas, *Geophys. Res. Lett.,23,* 1673, 1996.

Mandt, M. E., R. E. Denton, and J. F. Drake, Transition to whistler mediated magnetic reconnection, *Geophys. Res. Lett., 21* 73, 1994.

Parker, E. N., *J. Geophys. Res., 62,* 509, 1957.

Shay, M. A., J. F. Drake, R. E. Denton, D. Biskamp, Structure of the dissipation region during collisionless magnetic reconnection, *J. Geophys. Res., 103,* 9165, 1998.

Sweet, P. A., in Electromagnetic Phenomena in Cosmical Physics, edited by B. Lehnert (Cambridge University Press, New York, 1958), p. 123.

Vasyliunas, V. M., Theoretical models of magnetic field line merging, *Rev. Geophys. 13,* 303, 1975.

J. F. Drake and M. A. Shay, Institute for Plasma Research, University of Maryland, College Park, MD 20742. (email: drake@glue.umd.edu: shay@glue.umd.edu)